How to cite: *Angew. Chem. Int. Ed.* **2021**, *60*, 12132–12142
International Edition: doi.org/10.1002/anie.202103178
German Edition: doi.org/10.1002/ange.202103178

Self-Assembly

Three-Component Self-Assembly Changes its Course: A Leap from Simple Polymers to 3D Networks of Spherical Host–Guest Assemblies

*Eugenia Peresypkina, Kevin Grill[+], Barbara Hiltl[+], Alexander V. Virovets, Werner Kremer, Jan Hilgert, Wolfgang Tremel, and Manfred Scheer**

Dedicated to Professor Peter Klüfers on the occasion of his 70th birthday

Abstract: *One-pot self-assembly reactions of the polyphosphorus complex [Cp*Fe(η^5-P_5)] (**A**), a coinage metal salt $AgSbF_6$, and flexible aliphatic dinitriles $NC(CH_2)_xCN$ ($x = 1$–10) yield 1D, 2D, and 3D coordination polymers. The seven-membered backbone of the dinitrile was experimentally found as the borderline for the self-assembly system furnishing products of different kinds. At $x < 7$, various rather simple polymers are exclusively formed possessing either 0D or 1D Ag/**A** structural motifs connected by dinitrile spacers, while at $x \geq 7$, the self-assembly switches to unprecedented extraordinary 3D networks of nano-sized host–guest assemblies $(SbF_6)@[(\mathbf{A})_9Ag_{11}]^{11+}$ ($x = 7$) or $(\mathbf{A})@[(\mathbf{A})_{12}Ag_{12}]^{12+}$ ($x = 8$–10) linked by dinitriles. The polycationic nodes represent the first superspheres based on **A** and silver and are host–guest able. All products are characterized by NMR spectroscopy, mass spectrometry, and single-crystal X-ray diffraction. The assemblies $[(\mathbf{A})_{12}Ag_{12}]^{12+}$ were visualized by transmission electron microscopy.*

Introduction

In supramolecular chemistry the understanding of self-assembly processes is a challenge, and controlling such processes for practical purposes is an even more ingenious and skillful task. Such is the design of matrices for guest encapsulation and storage applicable in chemo sensing, drug delivery, and controlled absorption.[1] The manifold approaches in this research area investigated over the past years are conceptually based on either guest-oriented or host-oriented strategies. The first concept implies the fitting of the local environment to the guest molecules and therefore utilizes supramolecular host cages[2] and capsules[3] which are structurally tailored for the size and shape[4] of the guest or expediently functionalized[5] to facilitate host–guest interactions.[6] The second concept suggests furnishing extended space for guest molecules within the pores of the host and therefore uses microporous polymeric matrices,[7] or mesoporous materials.[8] To rationalize the design of infinite networks with the desired structure and function from pre-organized or self-assembled building blocks and linking units even new fields of research have emerged.[9] A combination of these approaches could have the best of both worlds, and the materials combining advantageous properties of finite capsules and of bulk porous materials could close this conceptual gap.

First approaches in this direction were demonstrated by the Atwood group.[10] Using self-assembly of pyrogallol-[4]arenes (L) as polydentate ligands with M^{II} salts (M^{II} = Cu, Ni, Mg), a series of crystalline 1D and 2D supramolecular coordination polymers (CPs) was obtained in which large metal–organic polyhedra $[M_{24}L_6]$ (MOP) represented the nodes, while the terminal groups of the same ligands L additionally join MOPs as linkers to give supramolecular CPs.[10] This elegant one-pot two-component self-assembly approach is however restricted to the ligands capable of such dual function. A straightforward one-pot reaction of a metal salt, a MOP-building ligand, and a spacer would be a desirable simplification on the synthetic route. However, to the best of our knowledge, no supramolecular CPs obtained in this way are reported. In many cases the polyhedral metal complexes have to be isolated first. Apparently, coordination polymers with nodes consisting of single metal cations or small compact metal complexes are formed instead or together with the desired supramolecular product. The pre-formed supramolecular nodes[11] are required to be activated for further direct polymerization,[11b,c] or spacing ligands have to be introduced in the second step.[11d,12] Besides inconvenient two-stage synthesis, their further polymerization often leads to amorphous products, a property which significantly complicates characterization of the product. Additionally, metal–organic polyhedra incorporated in supramolecular CPs could be

[*] Dr. E. Peresypkina, K. Grill,[+] Dr. B. Hiltl,[+] Dr. A. V. Virovets, Prof. Dr. M. Scheer
Institute of Inorganic Chemistry
University of Regensburg
93040 Regensburg (Germany)
E-mail: manfred.scheer@ur.de
Prof. Dr. W. Kremer
Institute of Biophysics and Physical Biochemistry
University of Regensburg
93040 Regensburg (Germany)
Dr. J. Hilgert, Prof. Dr. W. Tremel
Institute of Inorganic Chemistry and Analytical Chemistry
University of Mainz
55128 Mainz (Germany)
[+] These authors contributed equally to this work.
Supporting information and the ORCID identification number(s) for the author(s) of this article can be found under: https://doi.org/10.1002/anie.202103178.

enhanced if the MOPs possessed a functionality as for instance the targeted encapsulation of a guest, which is still a rare phenomenon in this area of supramolecular chemistry.[10f]

We have been successfully examining the host–guest properties of various spherical aggregates based on the polyphosphorus complexes $[Cp^{R}Fe(\eta^5\text{-}P_5)]$ ($Cp^{R} = Cp^{*}$(**A**), $Cp^{Bn} = (Cp(CH_2Ph)_5)$) and CuX or CuX_2 (X = Cl, Br, I, or triflate).[13] Their nano-sized inorganic scaffolds can contain eight to 24 *cyclo*-P_5 units and dozens of copper atoms or $\{Cu_nX_m\}$ fragments.[14] To use these supramolecular aggregates as hosting nodes joined in a polymeric structure it is necessary to provide coordination sites at the metal cations for the additional linkers, which should be longer than the van der Waals contact of the supramolecules. Moreover, the desired polymer of supramolecules should be accessible via a one-pot self-assembly. For this purpose we have chosen the silver salt with the non-coordinating anion SbF_6^-, which in the reaction with polyphosphorus ligand **A** would be able to form fullerene-like host–guest able supramolecules bearing free coordination sites at the silver centers. To link these in situ generated supramolecules, the flexible aliphatic dinitriles $NC(CH_2)_xCN$ (**DNx**, $x = 1$–10) were selected as their coordination chemistry with silver salts has already been investigated.[15]

Herein we report on a controllable three-component self-assembly system, leading either to CPs or to supramolecular CPs containing host–guest able nodes. During this study a phenomenon of the dramatic change of the self-assembly course from CP to supramolecular CP was discovered: For **DNx** with $x = 1$–6, the self-assembly leads to simple CPs, while starting from $x \geq 7$, the self-assembly suddenly leaps towards the formation of supramolecular CPs, only sporadically accompanied by CPs as minor products. The resulting supramolecular CPs are obtained in one-pot reactions in high yields and the supramolecular nodes are convenient for further implementation in host–guest chemistry.

Results and Discussion

Two-Component Self-Assembly

To prove that free coordination sites at silver cations can be generated, the two-component self-assembly of **A** and $AgSbF_6$ in both coordinating and non-coordinating solvents was investigated beforehand (Scheme 1). A solution of $AgSbF_6$ in CH_2Cl_2 was first layered with a mixture of CH_2Cl_2 and toluene (2:1) to prevent the formation of powder and then with a solution of **A** in toluene. After one day, dark-brown crystals of the 1D polymer $[(\mathbf{A})_2Ag]_n(SbF_6)_n$ (**I**) had formed. By changing the solvent of the Ag-containing layer to a mixture of CH_2Cl_2 and CH_3CN (2:1) and layering the fully diffused reaction solution with *n*-pentane, green plates of a dimeric $[(\mathbf{A})Ag(CH_3CN)_2]_2(SbF_6)_2$ complex (**II**) were obtained. The compounds **I** and **II** with 1:1 and 1:2 stoichiometric ratios of **A**:$AgSbF_6$, respectively, could be isolated in excellent crystalline yields.

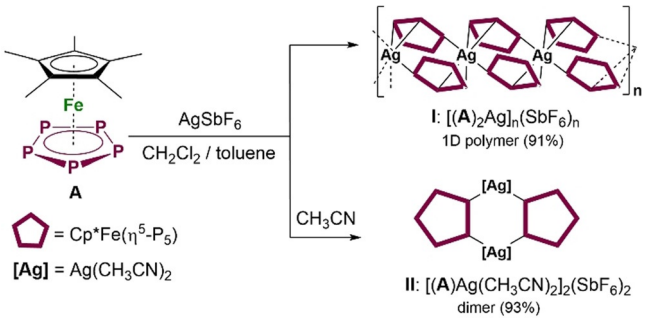

Scheme 1. Reactions of **A** with $AgSbF_6$ in different solvents. Isolated crystalline yields are given in parentheses.

According to the X-ray structure analysis, the *cyclo*-P_5 ligands in the 1D polymer **I** coordinate in a 1,2,3-mode to Ag atoms, which are pseudo-tetrahedrally coordinated by six P atoms of four *cyclo*-P_5 ligands of the units **A** (Figure 1a). The analogous cationic parts of **I** and of the earlier described 1D polymer $[(\mathbf{A})_2Ag]_n[Al\{OC(CF_3)_3\}_4]_n$[16] together with the related mass spectrometric and NMR spectroscopic features also suggest a monomer–oligomer equilibrium in solution.[17]

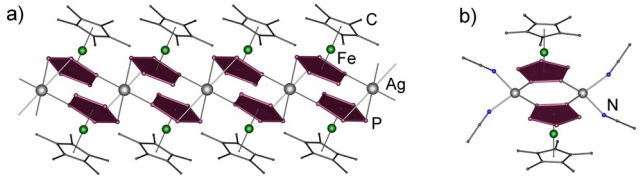

Figure 1. Structure of the cationic a) 1D polymer **I** and b) dimer **II**. H atoms are omitted for clarity.

Three-Component Self-Assembly

For three-component self-assembly reactions, a solution of $AgSbF_6$ in CH_2Cl_2 was layered with a mixture of CH_2Cl_2 and toluene and then with a toluene solution of **A** and the flexible **DNx** ($x = 1$–10). The selectivity of the reaction was controlled by using a reduced concentration of 2 mmol L^{-1} in the respective layers and an equimolar ratio of Ag:**A**. The corresponding dinitrile was added in a 10-fold excess with respect to **A**. Increasing the concentration of the Ag salt and **A** or decreasing the excess of dinitrile both yielded a 1D polymeric byproduct **I**. Combining the **DNx** and complex **A** in the toluene layer turned out to be decisive, because flexible aliphatic dinitriles readily react with Ag^+ to give insoluble polymeric products.[15f] However, these products turned out to be unavoidable in the case of shorter **DNx** ($x < 4$) even when using this precaution (see SI). Using the shortest dinitrile, dicyanomethane $NC(CH_2)CN$, a 2D polymer $[(\mathbf{A})_2Ag_3(\mathbf{DN1})_2(C_7H_8)]_n(SbF_6)_{3n}$ (**1**) is isolated selectively irrespective of the used stoichiometric ratios of **A**:$AgSbF_6$, which only influences the amount of the colorless byproduct $[Ag(\mathbf{DN1})](SbF_6)$, which can be separated manually (Scheme 2). For the dinitrile **DN2**, two polymeric products are formed as a mixture of 1D $[(\mathbf{A})Ag_2(\mathbf{DN2})_2]_n(SbF_6)_{2n}$ (**2a**: plates) and 2D $[(\mathbf{A})_2Ag_2(\mathbf{DN2})]_n(SbF_6)_{2n}$ (**2b**: needles) polymers accom-

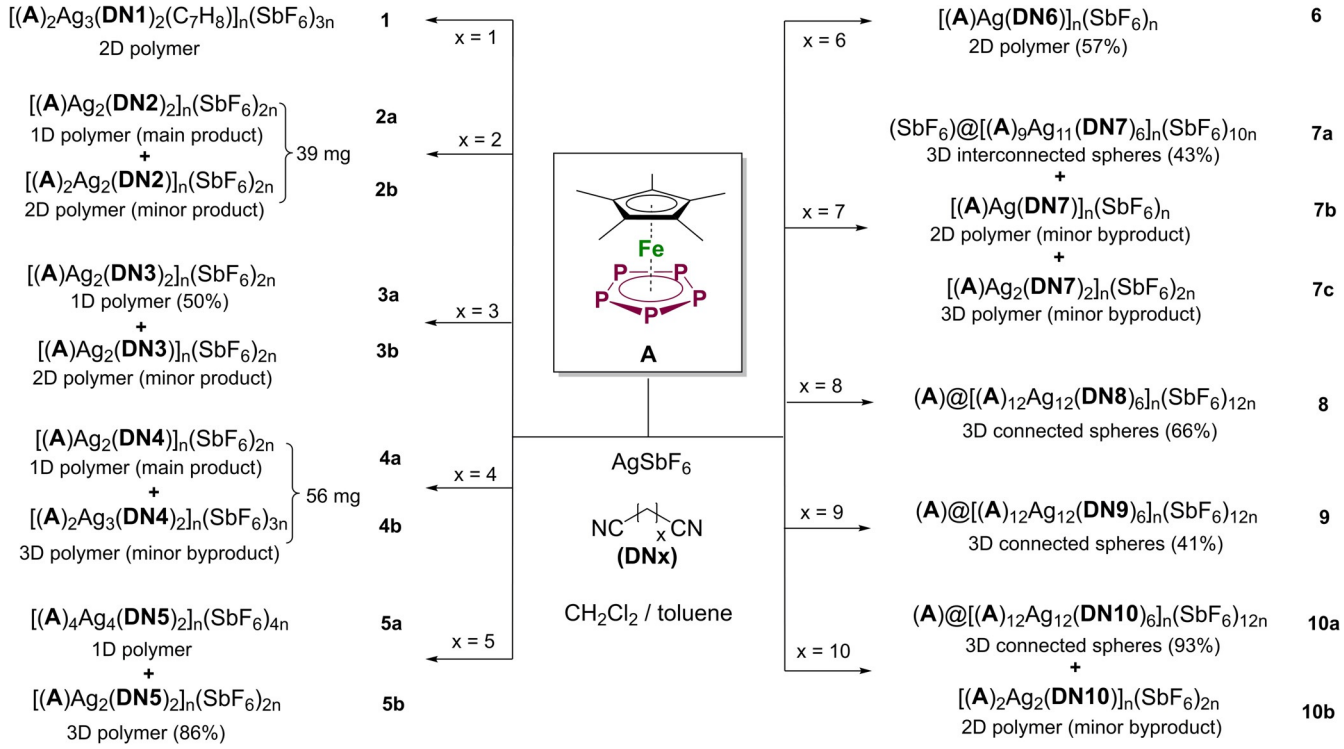

Scheme 2. One-pot self-assembly reactions of **A**, $AgSbF_6$, and flexible dinitriles **DNx**. Isolated crystalline yields are given in parentheses.

panied by small amounts of the **A**-free product [Ag(**DN2**)]-(SbF_6). Using **DN3** gives 1D $[(\mathbf{A})Ag_2(\mathbf{DN3})_2]_n(SbF_6)_{2n}$ (**3a**: plates) and a smaller amount of a 2D polymer $[(\mathbf{A})Ag_2(\mathbf{DN3})]_n(SbF_6)_{2n}$ (**3b**: prisms). The main product **3a** can be isolated selectively, while only few crystals of **3b** occur. Going further to **DN4**, a 2D polymer $[(\mathbf{A})Ag_2(\mathbf{DN4})]_n(SbF_6)_{2n}$ (**4a**) is accompanied by a few crystals of the first 3D polymer in the system **A**/$AgSbF_6$/**DNx** $[(\mathbf{A})_2Ag_3(\mathbf{DN4})_2]_n(SbF_6)_{3n}$ (**4b**) and by a small unavoidable impurity of [Ag(**DN4**)](SbF_6). With **DN5**, a 1D $[(\mathbf{A})_4Ag_4(\mathbf{DN5})_2]_n(SbF_6)_{4n}$ (**5a**) and a 3D $[(\mathbf{A})Ag_2(\mathbf{DN5})_2]_n(SbF_6)_{2n}$ (**5b**) polymer are obtained at 1:2 (mixture **5a** and **5b**) and at 1:1 (**5b**) stoichiometric ratios of **A**:$AgSbF_6$. Extending the linking unit to $x = 6$, a 2D polymer $[(\mathbf{A})Ag(\mathbf{DN6})]_n(SbF_6)_n$ (**6**) is formed selectively, irrespective of the used stoichiometric ratios of **A**:$AgSbF_6$. No phase transformation between major and minor products was observed when keeping under mother liquor solution (or freshly prepared solvent mixture of the same composition) for at least six months.

Going further to **DN7**, the system becomes versatile enough to form the unique representative of an unprecedented class of 3D supramolecular coordination polymers $[(SbF_6)@[(\mathbf{A})_9Ag_{11}(\mathbf{DN7})_6]]_n(SbF_6)_{10n}$ (**7a**) in which unique spherical aggregates, metal-*organometallic* polyhedra, act as nodes. This major product is accompanied by the 2D $[(\mathbf{A})Ag(\mathbf{DN7})]_n(SbF_6)_n$ (**7b**) and 3D $[(\mathbf{A})Ag_2(\mathbf{DN7})_2]_n(SbF_6)_{2n}$ (**7c**) CPs as minor byproducts. Though the stoichiometric ratios in **7a** to **7c** differ, they could not be isolated selectively, not even by using different stoichiometric ratios or different concentrations of the starting materials. For longer dinitriles with $x =$ 8 and 9, the formation of simple CPs was not observed. Instead, unprecedented 3D supramolecular CPs, the polymeric networks of supramolecular spherical aggregates $[(\mathbf{A})@\{(\mathbf{A})_{12}Ag_{12}(\mathbf{DNx})_6\}]_n(SbF_6)_{12n}$ ($x = 8$ (**8**), 9 (**9**), and 10 (**10a**)) were obtained in moderate to excellent crystalline yields (Scheme 2). Note that, in the case of **DN10**, the formation of the 1D CP **I** could not be impeded completely, along with the occasional formation of a few crystals of a 2D CP $[(\mathbf{A})_2Ag_2(\mathbf{DN10})]_n(SbF_6)_{2n}$ (**10b**) as the second minor byproduct. All crystalline compounds are differently tinted green-brown; the 2D polymeric compounds are often dichroic green-to-brown.

Simple Polymers Based on DNx with x = 1–7 and 10b

According to the X-ray diffraction, the simple polymers based on **A**, $AgSbF_6$, and flexible dinitriles possess 1D to 3D dimensionalities, with the variety arising from only two types of Ag/*cyclo*-P_5 subunits, finite (Figure 2a,b) and 1D chains (Figure 3–5), whereas 1D polymeric structural motifs can be additionally augmented by **DNx** (Figure 6). The types of the 0D nodes and 1D subunits are summarized in Table 1. The 0D motifs are only found for the **DN5**–**DN7** in case of a medium-length aliphatic chain, while 1D motifs occur for any **DNx** linker lengths. The overall dimensionality of the resulting structures seems to be governed by the ratio of the building blocks in the product rather than by the linker length as no clear tendency shows except that, with longer linkers, 3D structures (**DN4**–**DN7**) gradually outnumber the 1D polymeric motifs (**DN2**–**DN5**). However, 2D motifs dominate for all dinitriles with the exception of **DN5**, and

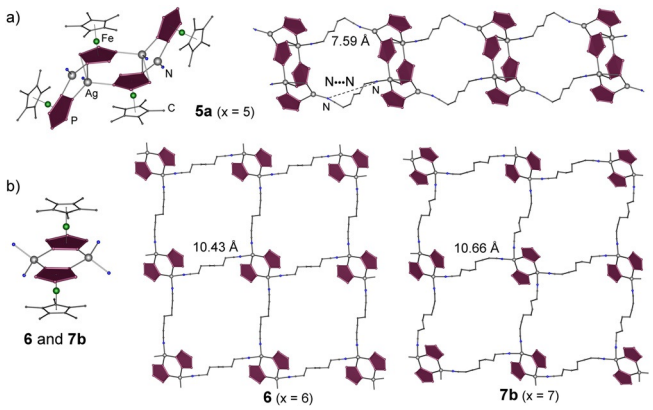

Figure 2. Structure of the cationic networks based on finite Ag—P fragments: a) tetrameric node of the 1D polymer in **5a** and b) dimeric node in the isotypic 2D networks **6** and **7b** including the intramolecular N···N contacts in dinitrile linkers. {Cp*Fe} fragments and H atoms are not shown.

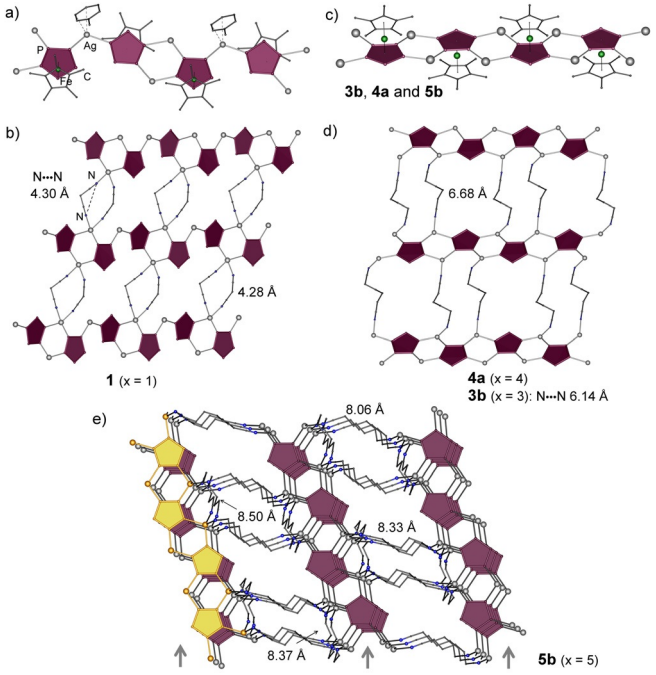

Figure 3. Structure of the cationic networks based on 1D Ag—P fragments: a,b) $[(\mathbf{A})_2Ag_3(C_7H_8)]_n^{3n+}$ in **1**; c) 1D strand $[(\mathbf{A})Ag_2]_n^{2n+}$ in the isotypic 2D layers of d) **3b** and **4a** as well as e) in a 3D network of **5b** including the intramolecular N···N contacts in linkers. {Cp*Fe} fragments and H atoms are not shown.

isotypic motifs occur quite at random (see below). The structures with the same ratio of **A**:Ag:**DNx** can demonstrate both similar and different connectivity depending on the various coordination modes of the pentaphosphaferrocene **A**.

The 2D network in **1** consists of parallel 1D strands $[(\mathbf{A})_2Ag_3]_n^{3n+}$ with *cyclo*-P_5 ligands of the units **A** coordinating Ag atoms in alternating 1,2,3- and 1,2,4-coordination modes (Table 1, Figure 3a). The strands are bridged by two angular dinitriles coordinating the same Ag atoms of the strand (Figure 3b). Interestingly, a toluene molecule is additionally

Table 1: Coordination modes and motifs in simple polymers.

Polymer[a]	Node[b]	**A**:Ag:**DNx**	*cyclo*-P_5 coordination	CN(Ag)[c]
1 (2D)	$[(\mathbf{A})_2Ag_3]_n^{3n+}$	2:3 : 2	1,2,3; 1,2,4	2P + 2N, 2P + 2C
2a (1D)	$[(\mathbf{A})Ag_2(\mathbf{DN2})_2]_n^{n+}$	1:2 : 2	1,2,3,4	2P + 2N
2b (2D)	$[(\mathbf{A})Ag]_n^{n+}$	2:2 : 1	1,2,3,4; 1,2	3P + 1N
3a (1D)	$[(\mathbf{A})Ag_2(\mathbf{DN3})_2]_n^{n+}$	1:2 : 2	1,2,3,4	2P + 2N
3b (2D)	$[(\mathbf{A})Ag_2]_n^{2n+}$	1:2 : 1	1,2,3,4	2P + 1N
4a (2D)	$[(\mathbf{A})Ag_2]_n^{2n+}$	1:2 : 1	1,2,3,4	2P + 1N
4b (3D)	$[(\mathbf{A})_2Ag_3]_n^{3n+}$	2:3 : 2	1,2,4	2P + 1N, 2P + 2N
5a (1D)	$[(\mathbf{A})_4Ag_4]^{4+}$	2:2 : 1	1,2	2P + 1N, 3P + 1N
5b (3D)	$[(\mathbf{A})Ag_2]_n^{2n+}$	1:2 : 2	1,2,3,4	2P + 2N
6 (2D)	$[(\mathbf{A})_2Ag_2]^{2+}$	1:1 : 1	1,2	2P + 2N
7b (2D)	$[(\mathbf{A})_2Ag_2]^{2+}$	1:1 : 1	1,2	2P + 2N
7c (3D)	$[(\mathbf{A})Ag_2(\mathbf{DN7})_{0.5}]_n^{2n+}$	1:2 : 2	1,2,3,4	3P + 1N
10b (2D)	$[(\mathbf{A})Ag]_n^{n+}$	2:2 : 1	1,2,3,4; 1,2	3P + 1N

[a] Dimensionality is given in parentheses. [b] *n* always corresponds to 1D motifs. [c] Coordination environment.

coordinated to a two-coordinate silver atom with Ag–C distances of 2.44(1)–2.62(1) Å. This feature makes **1** unique as all other compounds in the family possess no such interactions despite the fact that toluene is also used as a solvent and is often present in the crystal structures of these compounds as a solvate molecule. For the dinitrile **DN2**, the 1D polymer (**2a**) furnishes a chain of the *cyclo*-P_5 ligands coordinating Ag atoms in a 1,2,3,4-mode. The Ag ions are in turn tetrahedrally coordinated by pairs of dinitriles chelating neighboring Ag atoms of the same chain (Table S29, Figure 6a). Also a 2D motif (**2b**) is possible for this linker, which is based on the 1D polymeric bands $[(\mathbf{A})Ag]_n$ of *cyclo*-P_5 ligands in a 1,2,3,4-mode similar to the chains in **2a**, but, instead of two augmenting linkers, the neighboring Ag atoms are decorated additionally by a molecule **A** in a 1,2-coordination mode. The dinitriles connect the bands in a 2D network with identical trapezoidal meshes (Figure 4a,b).

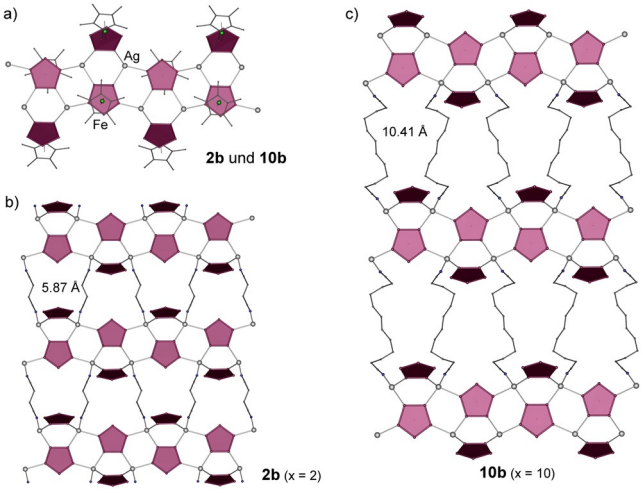

Figure 4. Structure of a) a 1D cationic motif $[(\mathbf{A})Ag]_n^{n+}$, b) a 2D polymer of isotypic **2b**, and c) **10b** including the intramolecular N···N contacts in dinitrile linkers. {Cp*Fe} and H atoms are omitted.

For the dinitrile **DN3**, the major product is a 1D polymer (**3a**) whose structure is similar to that in **2a** (Figure 6a), as the dinitrile ligands are only long enough to chelate Ag atoms coordinated to the positions 1 and 2 of the unit **A** within the strand giving rise to this augmented motif, which disappears for longer dinitriles. A 2D polymer (**3b**), a minor product in this reaction, is based on $[(\mathbf{A})Ag_2]_n^{2n+}$ strands in which *cyclo*-P_5 ligands of **A** coordinate in a 1,2,3,4-mode to Ag atoms being in a triangular environment.

For the linker **DN4**, a 2D polymer (**4a**) repeating the motif of **3b** is formed (Figure 3d) accompanied by a few crystals of a 3D polymer (**4b**). The latter shows a unique structure within its family being built up by puckered chains $[(\mathbf{A})_2Ag_3]_n^{3n+}$ with tetrameric repeating units (Figure 5). In each repeating unit, two opposed *cyclo*-P_5 ligands coordinate to Ag atoms in a 1,2,4-mode. The other two *cyclo*-P_5 ligands coordinate Ag atoms in a 1,2-mode and additionally form two longer π-contacts (2.83–2.93 Å). The Ag atoms possess either a trigonal or a distorted pseudo-tetrahedral coordination, the latter also including two π-contacts (Figure 5a). The dinitrile ligands connect parallel chains in a 3D polymeric structure (Figure 5c).

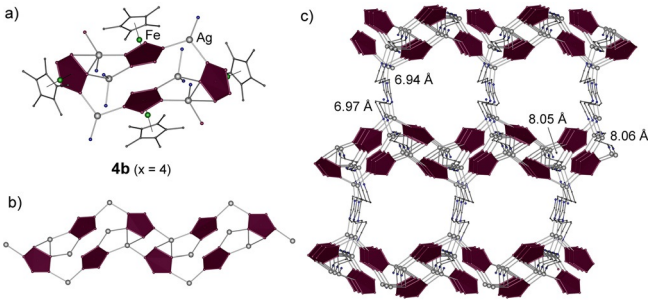

Figure 5. a) Repeating tetrameric unit; b) a 1D polymeric motif $[(\mathbf{A})_2Ag_3]_n^{3n+}$ connected in c) a 3D network in **4b**. {Cp*Fe} and H atoms are omitted.

The ladder-like 1D polymer in **5a** is built up by tetrameric units $[(\mathbf{A})_4Ag_4]^{4+}$ (Figure 2a). The Ag atoms show either a trigonal or a distorted pseudo-tetrahedral coordination. Two *cyclo*-P_5 ligands coordinate to Ag atoms in a 1,2-mode. The other two *cyclo*-P_5 ligands coordinate Ag atoms in a 1,3-mode and additionally form two longer π-contacts (2.80, 3.09 Å) with the opposing Ag atom similar to those in **4b** and $[(\mathbf{A})_2Ag]_n[Al\{OC(CF_3)_3\}_4]_n$ (2.80–2.81 Å).[16]

Another 3D network in the series is **5b** representing parallel 1D strands $[(\mathbf{A})Ag_2]_n^{2n+}$, the same as in **4a**, connected by dinitriles (Figure 3c,e). The strands are built up by 1,2,3,4-coordinated *cyclo*-P_5 ligands and Ag atoms, but, in contrast to **4a**, in a tetrahedral environment. The linkers connect each 1D strand to four other ones resulting in a 3D structure.

For the dinitrile **DN6**, the resulting 2D polymer **6** is built up by dimeric nodes $[(\mathbf{A})_2Ag_2]^{2+}$ (cf. dimer **II**), which are connected via the flexible linkers to give a square net (Figure 2b). Each *cyclo*-P_5 ligand coordinates in a 1,2-mode to tetrahedrally coordinated Ag atoms. A similar 2D framework is also formed in **7b**, a byproduct of the self-assembly of **A**, $AgSbF_6$, and **DN7**. In contrast to **6**, the dimeric nodes in **7b** are not parallel, but alternately turned about (Figure 2b). The 3D polymer **7c** is the other minor byproduct of the reaction with **DN7**. The 1D strands $[(\mathbf{A})Ag_2]_n^{2n+}$ are similar to those in **4a** and **5b**, but form alternating stacks. Moreover, the dinitrile ligands are sufficiently long to chelate Ag atoms coordinated to the positions 1 and 4 of the unit **A** belonging to the same strand thus forming another augmented motif than that for the shorter dinitriles **DN2** and **DN3**. Thereby, only half of the linkers connect the strands in a 3D network of **7c** (Figure 6b,c).

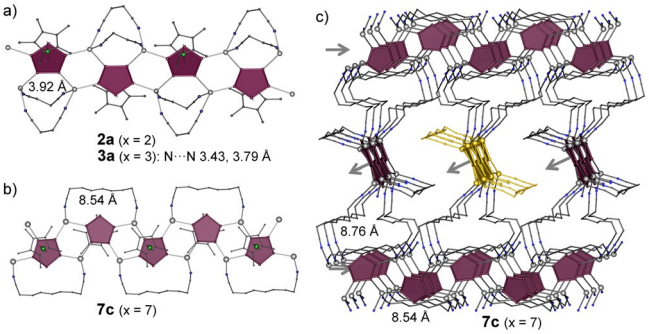

Figure 6. Structure of the cationic networks based on 1D Ag–P fragments augmented by dinitriles: a chain $[(\mathbf{A})Ag_2(\mathbf{DNx})_2]_n^{n+}$ in isotypic a) **2a** and **3a**; b) a strand $[(\mathbf{A})Ag_2(\mathbf{DN7})_{0.5}]_n^{2n+}$; c) 3D network of **7c** including the intramolecular N···N contacts within the linkers. {Cp*Fe} and H atoms are not shown.

The self-assembly with **DNx** ($x = 8, 9$) furnished no simple CPs (see below). In the minor byproduct **10b** of the self-assembly involving the **DN10**, a 2D polymeric framework of interconnected 1D strands $[(\mathbf{A})Ag]_n^{n+}$, unexpectedly repeats the structural motif previously observed for the **2b** structure, based on one of the shortest linkers, **DN2** (Figure 4).

3D Supramolecular Coordination Polymers

The discontinuous switch in the one-pot self-assembly of **A**, $AgSbF_6$, and flexible **DNx** starts at $x \geq 7$. The main product **7a** of the self-assembly between **A**, $AgSbF_6$, and **DN7** is the first representative of a novel class of 3D supramolecular CPs based on polyphosphorus ligands, being also the first example of a supersphere based on **A** and Ag (Figure 7). Here, unprecedented 56-vertex polycationic assemblies $[(\mathbf{A})_9Ag_{11}]^{11+}$ act as nodes. These nodes of C_s point symmetry possess the shape of a tricapped trigonal prism outlined by the centers of the P_5 rings. Nine *cyclo*-P_5 ligands show four different coordination modes (Figure 7c). The Ag atoms are tetrahedrally or pseudo-tetrahedrally coordinated (Table 2). The Ag–N bond lengths for the end-on coordination mode of the dinitriles amount to 2.19–2.34 Å, whereas the Ag–N bonds for the less common η^2-coordination are significantly elongated (2.95 and 3.20 Å), but still in agreement with literature data.[18]

The outer diameter of the spherical cationic assembly amounts to 2.21 nm,[20] which, to date, makes it the smallest

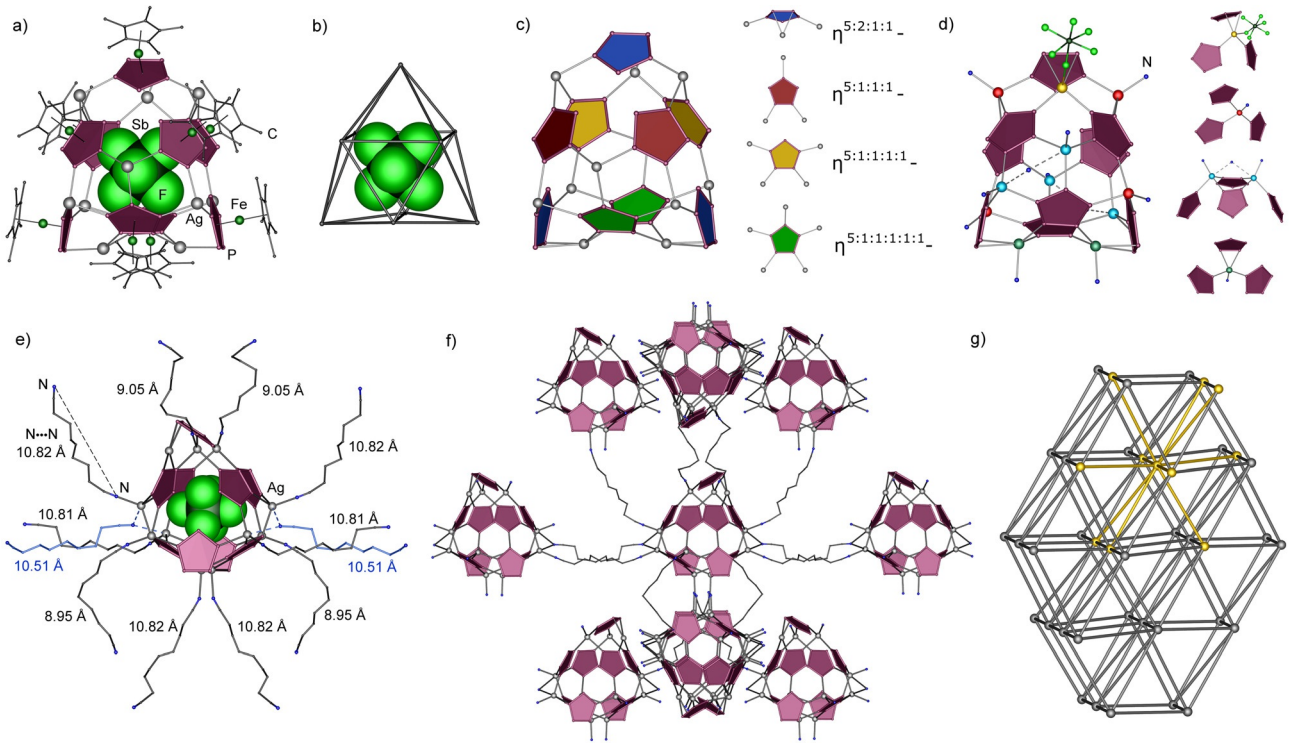

Figure 7. Polymer **7a** with supramolecular assemblies as nodes. a) The $(SbF_6)@[(\mathbf{A})_9Ag_{11}]^{10+}$ node; b) tricapped trigonal prism formed by the centers of the P_5 rings. Different coordination modes of c) the *cyclo*-P_5 ligands and d) the Ag atoms highlighted by color; e) the node with outgoing linkers; f) section of the 3D cationic network, also shown in yellow in g) simplified 10-connected overall network.

Table 2: Selected structural characteristics of **7a–10a**.

Compound	Node	Ag—P[a]	$Ø_{out}$[b]	$Ø_{in}$[b]	**DNx**[c]	linear **DNx**[d]
7a	$[(\mathbf{A})_9Ag_{11}]^{11+}$	2.40–2.61 (σ) 2.72–2.88 (π)	2.21	0.56	8.95–10.82	11.94
8	$[(\mathbf{A})_{12}Ag_{12}]^{12+}$	2.44–2.60	2.44	0.80	9.99–10.58	13.38
9	$[(\mathbf{A})_{12}Ag_{12}]^{12+}$	2.42–2.63	2.43	0.74	10.44–10.87	14.50
10a	$[(\mathbf{A})_{12}Ag_{12}]^{12+}$	2.48–2.55	2.40	0.83	10.75–11.99	15.90

[a] Range of bond distances (in Å). [b] Outer and inner diameter of the node, nm. [c] A range of the lengths of the **DNx** linkers in the respective crystal structure. [d] Calculated length of the **DNx** linkers in a linear conformation.[19]

spherical assembly based on the five-fold symmetric building block **A** along with the 80-vertex scaffold $[(\mathbf{A})_{12}(CuX)_{20}]$ (X = Cl, Br) of 2.29 nm.[14] Each supramolecular node acts also as a molecular container for an SbF_6^- counter-anion. The anion is ordered in a void of 0.56 × 0.60 nm with F atoms pointing in-between *cyclo*-P_5 ligands to avoid short intermolecular contacts. As a result, numerous F···P van der Waals contacts are formed in a range of 3.21–3.36 Å. The encapsulation of SbF_6^- shows that the nodes are capable of host–guest chemistry. The single-crystal X-ray structure analysis of **8–10a** also revealed the 3D supramolecular CPs of unique spherical polycationic nodes connected by dinitriles (Figure 8, Figure 9). However, in comparison to **7a**, the nodes show a completely different structure: The larger 72-vertex node $[(\mathbf{A})@(\mathbf{A})_{12}Ag_{12}]^{12+}$ consists of 12 units of **A**, which are

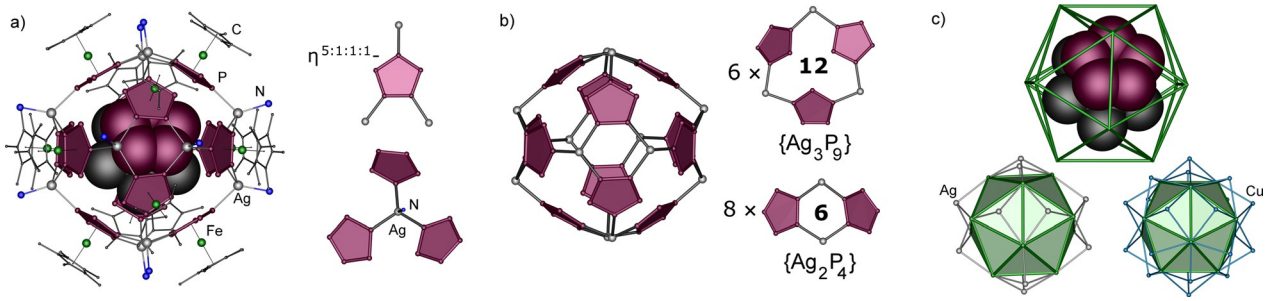

Figure 8. Supramolecular assemblies as nodes in the 3D networks **8–10a**. a) $[(\mathbf{A})@(\mathbf{A})_{12}Ag_{12}]^{12+}$ as nodes with the coordination mode of the *cyclo*-P_5 ligands and the Ag atoms; b) inorganic core based on 6- and 12-membered rings; c) icosahedron formed by centers of the P_5 rings and its variations with Ag and Cu caps.[14b]

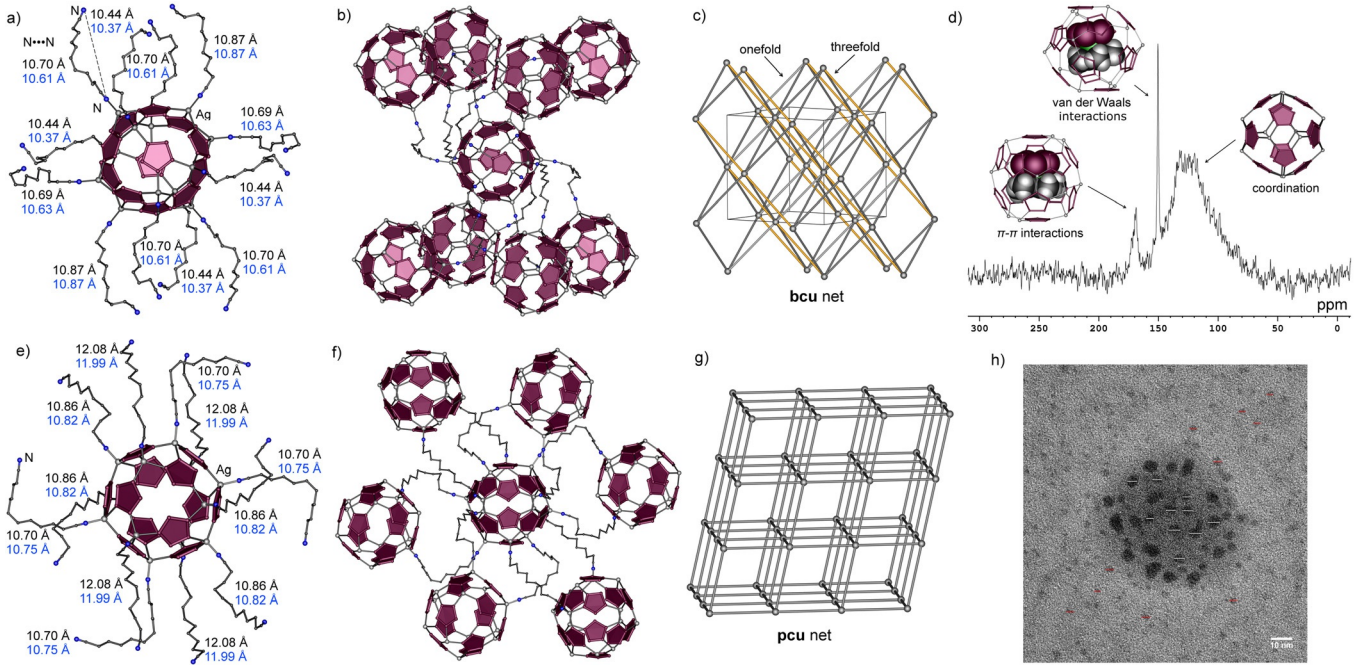

Figure 9. 3D Networks of supramolecular assemblies in **8**–**10a.** Node with 12 bridging linkers in a) **9** and e) **10a**; the lengths N···N at 100 K (black) and 10 K or 30 K (blue); a section of the 3D cationic network in b) **8** and f) **10a**; c) 8-connected underlying net in **8** and **9**; and g) 6-connected underlying net in **10a**; d) ^{31}P MAS NMR spectrum of **8**; and h) TEM record of **8** dispersed in CH_2Cl_2.

arranged in an icosahedron of 12 Ag atoms systematically capping 12 of the 20 available trigonal faces. The remaining eight faces give rise to 12-membered $\{Ag_3P_9\}$ rings in the inorganic scaffold (Figure 8b,c). Every *cyclo*-P_5 ligand coordinates to Ag atoms in a 1,2,4-mode, presenting the first spherical aggregate exclusively composed of three-coordinated units of **A**. The Ag atoms are tetrahedrally coordinated by three units of **A** and one dinitrile linker bridging two neighboring spheres (Figure 8a).

An icosahedral arrangement of 12 *cyclo*-P_5 units was also observed for the spherical supramolecules based on the *cyclo*-P_5 complexes and Cu halides $[(Cp^RFe(\eta^5\text{-}P_5))_{12}\{CuX\}_{20-n}]$ ($Cp^R = Cp^*$ (**A**), Cp^{Bn} (**B**); X = Cl, Br; n = 0–4.8).[13c,e,14b] Unlike Ag-based cationic nodes, the Cu-containing nodes are neutral, and all trigonal faces of an icosahedron are statistically capped with (20−n) CuX units (Figure 8c). However, in **8**–**10a**, owing to the coordination of dinitrile linkers, the 12 silver and exactly eight vacant positions in the cationic nodes are ordered. In addition, Ag-based cationic scaffolds are more flexible due to the more deformable coordination sphere of Ag as compared to Cu.[21] The Ag–P bond lengths vary in a wide range (Table 2). For this reason, the cationic nodes are geometrically distorted causing crystallographic disorder (see Supporting Information for details).

The IR spectra of crystals of **7a**–**10a** confirm the coordination of dinitriles to the Ag atoms, as the observed stretching mode of the nitrile group at $\tilde{\nu}$ = 2270 (**7a**), 2264 (**8**), 2269 (**9**), 2268 cm^{-1} (**10a**) is slightly blue-shifted compared to that of the free dinitriles at $\tilde{\nu}$ = 2247 cm^{-1}.

Each spherical node in **8**–**10a** of 2.07 × 2.44 nm encapsulates a molecule of **A** in the inner cavity of 0.79 × 0.97 nm (Figure 8a,c). Interestingly, similar Cu-based supramolecules $[(\mathbf{A})_{12}Cu_{20-n}]$ are slightly smaller (2.31 nm) due to shorter M–P bonds (Cu-P: 2.24–2.31 Å) and cannot incorporate a non-spherical molecule of **A** in their spherical cavity of Ø = 0.81 nm.[14b] Therefore, the encapsulation must be realized directly during the formation of this sphere. The guest molecule **A** in the cavity of the nodes is disordered over six positions so that the *cyclo*-P_5 unit in every orientation of the guest is opposite to the one of the six *cyclo*-P_5 rings of the node scaffold. The flexibility of the Ag coordination environment[21] allows the scaffold to adjust to the shape of the guest molecule: It is slightly elongated in the direction of the axis of the guest molecule **A** to 2.44 nm and narrowed to 2.07 nm in other directions (cf. SI for details).[20] Such adjustability of the core is also favored by the lower denticity of the pentaphosphaferrocene units, showing that the encapsulation of the guest occurs simultaneously during the formation process of the sphere and the linkage to other units.

Depending on the orientation of the guest **A**, different host–guest interactions occur. In two of the six orientations, the P_5 ring of the guest is parallel to two of the P_5 rings of the host (**8**: 0.1(2)° and **9**: 0.3(2)°). The corresponding interplanar *cyclo*-P_5(guest)···*cyclo*-P_5(host) distances of 3.79(1) (**8**) and 3.80(1) Å (**9**) point to rather weak π–π interactions (cf. SI). In other orientations of the guest molecule **A**, the *cyclo*-P_5 planes are inclined by 3.2(5)–8.5(1)° (**8**) and 3.3(2)–9.5(1)° (**9**), suggesting only van der Waals host–guest interactions. In all positions of the guest in **10a**, one can suggest only slightly inclined orientations of the P_5 rings of the guest and the host (1.8(5)–4.6(5)°) with interplanar distances of 3.68(2)–3.82(1) Å.

Remarkably, the supramolecular CPs do not show decomposition being stored in a glovebox, and can be kept under mother liquor solution for six months or longer. Only if exposed to the air, or upon changes of mother liquor solution composition, a degradation of **7**–**10a** takes place to give **I** and presumably corresponding colorless **A**-free compound of silver and dinitrile.

Solid State NMR Study for the Supramolecular CP 8

To additionally investigate host–guest interactions in the solid state, a ^{31}P MAS NMR measurement was exemplified for one of the two isotypic compounds, namely **8** (Figure 9d), with a broad signal at 125 ppm with an integral intensity of 60 being observed (half width $\tilde{\omega} \approx 5800$ Hz), which can most likely be attributed to the P atoms of the core.

The width of the signal agrees with the deformable coordination sphere of Ag. Two respective sharp signals at 150 ppm and 169 ppm with integral intensities of approximately 2.5 can be attributed to the different orientations of the guest molecules **A** in the host scaffold. The signal at 150 ppm being close to the signal of the free complex **A** (149 ppm) can be assigned to the guest molecule **A** participating in weak van der Waals interactions with the host. The signal at 169 ppm, downfield shifted to the signal of the free complex **A**, resembles the chemical shift in the ^{31}P MAS NMR spectrum of the molecule **A** encapsulated in a 90-vertex supramolecule $[(\mathbf{A})_{12}(CuCl)_{25}(CH_3CN)_{10}]$ (X = Cl, Br) (160 ppm) featuring weak π–π interactions between *cyclo*-P_5 ligands of the host and the guest.[22] The corresponding geometry of the $P_5\cdots P_5$ interactions with interplanar distances of 3.86–4.03 Å and angles $< 0.9°$ is in good agreement with the one observed in **8**.[22] The same should be valid for **9** due to its close crystallographic similarity with **8**.

The 3D Supramolecular CP Network Topologies in 7a–10a

The 10-connected network of $[(\mathbf{A})_9Ag_{11}]^{11+}$ assemblies in **7a** can be topologically classified[23] as **bcu-*x*-10-Fmmm**.[9c] Each supramolecular node is linked to ten others via 12 dinitrile ligands: single connections with eight neighbors and double connections with two neighbors (Figure 7e,f). Two additional η^2-coordinated dinitrile linkers per node facilitate these double connections.

The polymeric networks formed by $[(\mathbf{A})_{12}Ag_{12}]^{12+}$ assemblies are isotypic for **8** and **9**, but differ for **10a**. Each sphere in **8** or **9** is connected via 12 dinitrile ligands to eight neighboring spheres: six of them are 1- and two are 3-connected (Figure 9a–c). The triple connections form parallel layers, which are spanned and joined together by the single connections to give the 8-connected nets assigned[23] to the **bcu**[9c] topology (body-centred cubic, Figure 9c). In contrast, each sphere in **10a** is connected to six others via 12 of the longest linkers, each pair of nodes being 2-connected. The respective topology of the underlying net is primitive cubic (**pcu**, Figure 9g).[9c,23]

In the crystal, the dinitrile linkers are folded by 9–20% (**7a**), 21–25% (**8**), 25–29% (**9**), and 28–33% (**10a**) which is illustrated by shortened intramolecular N···N distances compared to the corresponding linear conformation of the **DNx** molecules (Figure 9a,e, Table 2). This fact demonstrates the increasing folding of the higher homologs of the **DNx**.

To understand the nature of the crystallographic disorder in these highly disordered structures, X-ray diffraction studies at 100 and 10 K were performed for **9**, as well as at 90 and 30 K for **10a**. The guest molecules, the scaffold, linkers, and SbF_6^- anions stay positionally disordered even at temperatures as low as 10 K, pointing out the static nature of the disorder. The cooling to 10–30 K leads to the additional non-uniform shortening of the dinitrile units only by 0.06–0.09 Å (see SI, Table S28).

Transmission Electron Microscopy (TEM) Studies

TEM studies for compound **8** were conducted (Figure 9h). As the solid **8** is not soluble, but only dispersable in polar solvents such as CH_2Cl_2 after ultrasonication, it is not expected to give an isotropic distribution of the individual spherical nodes. **8** contains 12-fold positively charged organometallic cores and SbF_6^- counterions, held together by weak electrostatic interactions due to their low charge densities. Unlike neutral metal or metal oxide nanoparticles (e.g. Ag or Fe_3O_4), the cores of **8** are not protected by capping ligands and, hence, the building units of **8** are prone to aggregation, and therefore the TEM images show smaller and larger aggregates. The smallest aggregates have mean diameters between 3.1 (red bars) and 4.5 nm (white bars), each of them larger than the maximal dimension of 2.44 nm for the individual spherical node. Larger aggregates were observed by scanning probe microscopy (SPM). As the small aggregates, which are formed by evaporation of the dispersion medium during TEM sample preparation, are not well defined, "irregular spheres" appear in the projected view of a TEM image. EDX analysis of the particles gives an Ag:Fe ratio of approx. 1:1 as expected from the experimentally found metal ratio.

The Effect of the Linker Length

The length variation of the **DNx** linker ($x = 1$–10) does not significantly influence the connectivity of the resulting CPs but, at $x = 7$, discontinuously switches the three-component self-assembly of **A**, the coinage metal salt of a weakly coordinating anion $AgSbF_6$ and aliphatic dinitrile, from simple CPs at $1 < x < 6$ to the unprecedented 3D supramolecular CPs **7a**, **8**, **9**, and **10a** at $x \geq 7$. Remarkably, the tendency to form supramolecular CPs is so strong that it requires no change to the self-assembly system such as the delivery of a special template molecule,[21b] since the templating ion (SbF_6^- in **7a**) or a molecule (**A** in **8**–**10a**) are always present in the system and therefore cannot be the driving force behind such an unusual behavior in self-assembly.

Although the simple CPs still occur with **DN7** and **DN10** as minor products, the main pathway of the self-assembly is dominated by the formation of supramolecular CPs, the novel class of organometallic compounds. After the borderline $x = 7$, the simple CPs **7b**, **7c**, and **10b** suddenly become minor products despite their structural similarities to **6**, **4a** (and **5b**), and **2b**, respectively, being major products in the respective reactions. This fact can be explained by the conformation of the flexible linkers and their effective lengths (specified by the intramolecular distances N···N). In the 3D polymers **5b** and **6c** based on similar infinite strands $[(\mathbf{A})Ag_2)]^{2+}$, the crosslinking dinitriles possess comparable effective N···N lengths of 8.06–8.50 Å for **5b** and 8.76 Å for **7c**, though their aliphatic backbone differs by two CH_2 groups. In the similar 2D networks **5** and **6b**, the actual lengths of the linkers with the respective **DN6** and **DN7** are even closer-spaced, namely 10.43 Å (**6**) and 10.66 Å (**7b**). The formation of simple CPs at $x \geq 7$ might be hindered as the folding of the aliphatic chains is unfavorable for x smaller than 11–17.[24] However, one can see from Table 2 that the effective linker length for $x = 7$–10 grows slower than the calculated length of the linear **DNx** molecules (see SI for more details).

For the 3D supramolecular CP **7a** (Figure 7e), eight of the 12 **DNx** linkers are longer than or comparable in length (10.81–10.82 Å) to any of the lower homologs **DNx** in a linear conformation (9.39 ($x = 5$) and 10.88 Å ($x = 6$)). Similar linker lengths are observed for 3D networks connected with the **DNx**, $x = 8$, 9, and 10, which are not effectively longer than in **7a**. Such linker lengths (> 10.4–10.5 Å as compared with the effective linker length 10.44 Å in the last simple CP **6**) might be necessary for accommodating ten SbF_6^- anions that compensate the charge of a polycationic node in the outer sphere, which is not the case for the CPs with simple mono- to tetracationic nodes. Moreover, the longer length ensures reasonable van der Waals contacts between the spheres. Interestingly, for the 3D supramolecular CPs ($x \geq 7$), a tendency to a lower connectivity of the network with the elongation of the flexible dinitrile linker becomes evident: a 10-connected network in **7a**, an 8-connected network in **8** and **9**, and a 6-connected network in **10a**.

As **DN8** and **DN9** do not afford simple polymers, only linker lengths in the supramolecular CP **10a** and the CP **10b** can be compared (Table 2). On average, the linkers in CP **10b** (11.41 Å) are longer than in the supramolecular CP **10a** (av. 11.19 Å), the latter showing a wider range of 10.75–11.99 Å **DN10** length variation (Table 2). However, **DN10** linkers are significantly folded (cf. 15.9 Å in linear conformation, Table S28).

Obviously, some architectures are realized due to more specific tendencies. In this way, the augmented motifs in **2a**, **3a**, and suddenly again in **7c** occur when linker length and conformation become complementary to the Ag···Ag distance between coordinated Ag atoms first at 1,2-positions at the *cyclo*-P_5 ligands of **A** (5.0–5.3 Å for **DN2** and **DN3**) or at the 1,4-positions (8.1–8.2 Å for **DN7**). The most striking similarity of the networks is in **2b** and **10b** despite the difference of eight CH_2-groups in the linker backbones, demonstrating almost twice the expansion of the resulting 2D layers. This exemplifies that the simple expansion of the 2D network is irrelevant to the **DNx** folding and is stabilized by it. However, the CP **10b** is obtained in much lower yields than **2b**, overruled by the preferred formation of the supramolecular CP **10a**.

Characterization of 1–10 in Solution

While the compounds **I** and **II** are moderately soluble in CH_2Cl_2, the polymers **1**–**10b** are insoluble in hexane, toluene, CH_2Cl_2, thf, and Et_2O. Yet, all compounds readily dissolve in CH_3CN or pyridine at the cost of the degradation of the coordination network as well as of the supramolecular architecture and nodes. Therefore, in the ^1H, ^{13}C, ^{31}P, and $^{31}P\{^1H\}$ NMR spectra of the polymers treated by CD_2Cl_2/pyridine, only signals attributed to the free complex **A** and the dinitriles are detectable (cf. SI for details).

The peaks in the positive- and negative-ion mode of the ESI MS spectra correspond to various oligomeric fragments. The largest three-component fragments in the positive-ion mode for **I** or **1** can be assigned at $m/z = 798.9$ to a monocation $[(\mathbf{A})_2Ag]^+$. The peak at $m/z = 2869.1$ corresponds to $[(\mathbf{A})_5Ag_4(SbF_6)_3]^+$ for **II**, at $m/z = 2176$ to $[(\mathbf{A})_3Ag_4(SbF_6)_3]^+$ for **2**, at $m/z = 2519.8$ to $[(\mathbf{A})_3Ag_5(SbF_6)_4]^+$ for **3a**, and at $m/z = 2178.2$ to $[(\mathbf{A})_4Ag_3(SbF_6)_2]^+$ for **4**. The largest three-component fragments at $m/z = 2077.0$ and $m/z = 2426.0$ were identified as $[(\mathbf{A})_3Ag_3(SbF_6)_2(\mathbf{DN5})_2]^+$ and $[(\mathbf{A})_3Ag_3(SbF_6)_4(\mathbf{DN5})]^-$ (**5a**), $m/z = 2418.2$ and $m/z = 2772.0$ to $[(\mathbf{A})_3Ag_4(SbF_6)_3(\mathbf{DN5})_2]^+$ and $[(\mathbf{A})_4Ag_3(SbF_6)_4(\mathbf{DN5})]^-$ (**5b**), $m/z = 1622.4$ to $[(\mathbf{A})_2Ag_3(SbF_6)_2(\mathbf{DN6})]^+$ (**6**). In the ESI MS spectra of **7a**, **8**–**10**, oligomeric fragments can be detected and assigned at $m/z = 1636.6$ as $[(\mathbf{A})_2Ag_3(SbF_6)_2(\mathbf{DN7})]^+$ (**7a**), $m/z = 3729$ for $[(\mathbf{A})_9Ag_2(\mathbf{DN8})(SbF_6)]^+$ (**8**) and $m/z = 2521.98$ or 2522.0 for $[(\mathbf{A})_4Ag_4(SbF_6)_3]^+$ for **9** or for **10a**.

Conclusion

For the first time, 3D supramolecular CP networks built up by nano-sized organometallic Ag-based spherical aggregates, ready for host–guest interactions, were systematically obtained using the control of linker lengths. Utilizing the weakly coordinating anion SbF_6^- along with the five-fold symmetric building block pentaphosphaferrocene [Cp*Fe(η^5-P_5)] (**A**), and Ag^+, the predesigned free coordination sites on the Ag ion make the coordination by N-donor linkers possible. A detailed and systematic study on the three-component self-assembly of these building blocks and flexible linkers $NC(CH_2)_xCN$ (**DNx**, $x = 1$–10) showed that the variability of the conformations and thus the adjustable lengths of the linkers lead to the formation of diverse 1D to 3D coordination polymers. As a result, with **DNx** ($x = 1$–6), rather simple CPs are observed. With $x = 7$, the flexibility of the system brings it to a qualitatively novel level of aggregation and allows the formation of the first representative of an unprecedented spherical host scaffold, the 56-vertex polycationic host–guest assembly $(SbF_6^-)@[(\mathbf{A})_9Ag_{11}]^{11+}$, connected in a 3D supramolecular coordination polymer **7a**. When even longer linkers (**DN8**–**10**) are used, the self-

assembly system again switches to larger nano-sized supramolecular 72-vertex nodes of supramolecular CPs (**A**)@-$[(\mathbf{A})_{12}Ag_{12}]^{12+}$ serving as containers for the host molecules of **A**. Thus, two isotypic and one unique 3D supramolecular CPs $[(\mathbf{A})@\{(\mathbf{A})_{12}Ag_{12}(\mathbf{DNx})_6\}]_n(SbF_6)_{12n}$ ($x = 8$ (**8**), 9 (**9**), and 10 (**10a**)) were selectively isolated and structurally characterized. Moreover, for the first time, despite the insolubility of the supramolecular networks, by using TEM techniques, the visualization of giant spherical subunits was possible.

The ability of the three-component system to self-assemble in spherical polyphosphorus supramolecules over simple polymers in the absence of additional stimuli reveals immense perspectives arising from the combination of the assemblies readily offering host–guest chemistry with the advantages of 3D networks and their use in diverse applications. Based on our previous experience, targeted guest encapsulation seems also feasible, which offers the next step in this research and opens wide perspectives in tailoring the structure and property of the supramolecular nodes.

Acknowledgements

This work was supported by the Deutsche Forschungsgemeinschaft (DFG, project Sche 384/44-1). Parts of this research (projects I-20160654, I-20180967) were carried out at PETRA III, DESY, a member of the Helmholtz Association (HGF). We thank Dr. A. Burkhardt, Dr. O. Lorbeer and Dr. S. Panneerselvam for their assistance regarding the use of the beamline P11, as well as Dr. M. Tolkiehn for his assistance regarding the use of the beamline P24 at PETRA III, DESY. Open access funding enabled and organized by Projekt DEAL.

Conflict of interest

The authors declare no conflict of interest.

Keywords: coordination networks · flexible linkers · metallosupramolecular chemistry · pentaphosphaferrocene · supramolecules

[1] T. R. Cook, Y.-R. Zheng, P. J. Stang, *Chem. Rev.* **2013**, *113*, 734 – 777.

[2] a) M. Mastalerz, *Acc. Chem. Res.* **2018**, *51*, 2411 – 2422; b) M. De Rosa, P. La Manna, C. Talotta, A. Soriente, C. Gaeta, P. Neri, *Front. Chem.* **2018**, *6*, 84; c) Q. Shi, M. P. Mower, D. G. Blackmond, J. Rebek, Jr., *Proc. Natl. Acad. Sci. USA* **2016**, *113*, 9199 – 9203; d) P. Ballester, M. Fujita, J. Rebek, Jr., *Chem. Soc. Rev.* **2015**, *44*, 392 – 393; e) A. Granzhan, C. Schouwey, T. Riis-Johannessen, R. Scopelliti, K. Severin, *J. Am. Chem. Soc.* **2011**, *133*, 7106 – 7115; f) W. Meng, A. B. League, T. K. Ronson, J. K. Clegg, W. C. Isley, D. Semrouni, L. Gagliardi, C. J. Cramer, J. R. Nitschke, *J. Am. Chem. Soc.* **2014**, *136*, 3972 – 3980.

[3] Y. Inokuma, M. Kawano, M. Fujita, *Nat. Chem.* **2011**, *3*, 349 – 358.

[4] a) M. Otte, *ACS Catal.* **2016**, *6*, 6491 – 6510; b) F. J. Rizzuto, L. K. S. von Krbek, J. R. Nitschke, *Nat. Rev. Chem.* **2019**, *3*, 204 – 222; c) A. Granzhan, T. Riis-Johannessen, R. Scopelliti, K. Severin, *Angew. Chem. Int. Ed.* **2010**, *49*, 5515 – 5518; *Angew. Chem.* **2010**, *122*, 5647 – 5650; d) G. Liu, M. Zeller, K. Su, J. Pang, Z. Ju, D. Yuan, M. Hong, *Chem. Eur. J.* **2016**, *22*, 17345 – 17350.

[5] a) S. J. Barrow, S. Kasera, M. J. Rowland, J. del Barrio, O. A. Scherman, *Chem. Rev.* **2015**, *115*, 12320 – 12406; b) C. J. Hastings, M. D. Pluth, R. G. Bergman, K. N. Raymond, *J. Am. Chem. Soc.* **2010**, *132*, 6938 – 6940.

[6] K. Rissanen, *Chem. Soc. Rev.* **2017**, *46*, 2638 – 2648.

[7] a) E. T. C. Vogt, G. T. Whiting, A. D. Chowdhury, B. M. Weckhuysen in *Advances in Catalysis*, *Vol. 58* (Ed.: F. C. Jentoft), Elsevier, Amsterdam, **2015**, pp. 143 – 314; b) N. Jiang, R. Shang, S. G. J. Heijman, L. C. Rietveld, *Water Res.* **2018**, *144*, 145 – 161; c) L. Bacakova, M. Vandrovcova, I. Kopova, I. Jirka, *Biomater. Sci.* **2018**, *6*, 974 – 989; d) I. Stassen, N. Burtch, A. Talin, P. Falcaro, M. Allendorf, R. Ameloot, *Chem. Soc. Rev.* **2017**, *46*, 3185 – 3241; e) L. Wang, M. Zheng, Z. Xie, *J. Mater. Chem. B* **2018**, *6*, 707 – 717; f) L. Zhu, X.-Q. Liu, H.-L. Jiang, L.-B. Sun, *Chem. Rev.* **2017**, *117*, 8129 – 8176; g) X. Yang, Q. Xu, *Cryst. Growth Des.* **2017**, *17*, 1450 – 1455.

[8] A. E. Seitz, F. Hippauf, W. Kremer, S. Kaskel, M. Scheer, *Nat. Commun.* **2018**, *9*, 361.

[9] a) K. E. Cordova, O. M. Yaghi, *Mater. Chem. Front.* **2017**, *1*, 1304 – 1309; b) C. S. Diercks, Y. Liu, K. E. Cordova, O. M. Yaghi, *Nat. Mater.* **2018**, *17*, 301 – 307; c) M. O'Keeffe, M. A. Peskov, S. J. Ramsden, O. M. Yaghi, *Acc. Chem. Res.* **2008**, *41*, 1782 – 1789.

[10] a) C. Zhang, F. Wang, R. S. Patil, C. L. Barnes, T. Li, J. L. Atwood, *Chem. Eur. J.* **2018**, *24*, 14335 – 14340; b) R. M. McKinlay, G. W. V. Cave, J. L. Atwood, *Proc. Natl. Acad. Sci. USA* **2005**, *102*, 5944 – 5948; c) C. Zhang, R. S. Patil, C. Liu, C. L. Barnes, J. L. Atwood, *J. Am. Chem. Soc.* **2017**, *139*, 2920 – 2923; d) A. V. Mossine, C. M. Mayhan, D. A. Fowler, S. J. Teat, C. A. Deakyne, J. L. Atwood, *Chem. Sci.* **2014**, *5*, 2297 – 2303; e) L. Shao, B. Hua, X. Hu, D. Stalla, S. P. Kelley, J. L. Atwood, *J. Am. Chem. Soc.* **2020**, *142*, 7270 – 7275; f) D. A. Fowler, A. V. Mossine, C. M. Beavers, S. J. Teat, S. J. Dalgarno, J. L. Atwood, *J. Am. Chem. Soc.* **2011**, *133*, 11069 – 11071.

[11] a) E.-S. M. El-Sayed, D. Yuan, *Chem. Lett.* **2020**, *49*, 28 – 53; b) X.-Y. Xie, F. Wu, X. Liu, W.-Q. Tao, Y. Jiang, X.-Q. Liu, L.-B. Sun, *Chem. Commun.* **2019**, *55*, 6177 – 6180; c) G. Lal, M. Derakhshandeh, F. Akhtar, D. M. Spasyuk, J.-B. Lin, M. Trifkovic, G. K. H. Shimizu, *J. Am. Chem. Soc.* **2019**, *141*, 1045 – 1053; d) A. Carné-Sánchez, G. A. Craig, P. Larpent, T. Hirose, M. Higuchi, S. Kitagawa, K. Matsuda, K. Urayama, S. Furukawa, *Nat. Commun.* **2018**, *9*, 2506.

[12] a) H. Jung, D. Moon, H. Chun, *Bull. Korean Chem. Soc.* **2011**, *32*, 2489 – 2492; b) M. L. Schneider, O. M. Linder-Patton, W. M. Bloch, *Chem. Commun.* **2020**, *56*, 12969 – 12972.

[13] a) E. Peresypkina, C. Heindl, A. Virovets, H. Brake, E. Mädl, M. Scheer, *Chem. Eur. J.* **2018**, *24*, 2503 – 2508; b) J. Bai, A. V. Virovets, M. Scheer, *Science* **2003**, *300*, 781 – 783; c) F. Dielmann, M. Fleischmann, C. Heindl, E. V. Peresypkina, A. V. Virovets, R. M. Gschwind, M. Scheer, *Chem. Eur. J.* **2015**, *21*, 6208 – 6214; d) C. Schwarzmaier, A. Schindler, C. Heindl, S. Scheuermayer, E. V. Peresypkina, A. V. Virovets, M. Neumeier, R. Gschwind, M. Scheer, *Angew. Chem. Int. Ed.* **2013**, *52*, 10896 – 10899; *Angew. Chem.* **2013**, *125*, 11097 – 11100; e) A. Schindler, C. Heindl, G. Balazs, C. Groeger, A. V. Virovets, E. V. Peresypkina, M. Scheer, *Chem. Eur. J.* **2012**, *18*, 829 – 835; f) M. Scheer, A. Schindler, R. Merkle, B. P. Johnson, M. Linseis, R. Winter, C. E. Anson, A. V. Virovets, *J. Am. Chem. Soc.* **2007**, *129*, 13386 – 13387; g) C. Heindl, E. Peresypkina, A. V. Virovets, I. S. Bushmarinov, M. G. Medvedev, B. Kraemer, B. Dittrich, M. Scheer, *Angew. Chem. Int. Ed.* **2017**, *56*, 13237 – 13243; *Angew. Chem.* **2017**, *129*, 13420 – 13426.

[14] a) "Inorganic superspheres": E. Peresypkina, C. Heindl, A. V. Virovets, M. Scheer in *Clusters—Contemporary Insight in*

Structure and Bonding, *Vol. 174* (Ed.: S. Dehnen) Springer, Cham, **2016**, pp. 321 – 373; b) M. Scheer, A. Schindler, C. Gröger, A. V. Virovets, E. V. Peresypkina, *Angew. Chem. Int. Ed.* **2009**, *48*, 5046 – 5049; *Angew. Chem.* **2009**, *121*, 5148 – 5151; c) C. Heindl, E. V. Peresypkina, A. V. Virovets, W. Kremer, M. Scheer, *J. Am. Chem. Soc.* **2015**, *137*, 10938 – 10941.

[15] a) M. Elsayed Moussa, S. Evariste, B. Krämer, R. Reau, M. Scheer, C. Lescop, *Angew. Chem. Int. Ed.* **2018**, *57*, 795 – 799; *Angew. Chem.* **2018**, *130*, 803 – 807; b) M. Elsayed Moussa, B. Attenberger, E. V. Peresypkina, M. Fleischmann, G. Balázs, M. Scheer, *Chem. Commun.* **2016**, *52*, 10004 – 10007; c) A. Lennartson, P. Southon, N. F. Sciortino, C. J. Kepert, C. Frandsen, S. Morup, S. Piligkos, C. J. McKenzie, *Chem. Eur. J.* **2015**, *21*, 16066 – 16072; d) K. Chainok, W. Saphu, P. Khemthong, D. J. Harding, *Z. Anorg. Allg. Chem.* **2013**, *639*, 2134 – 2137; e) A. Westcott, N. Whitford, M. J. Hardie, *Inorg. Chem.* **2004**, *43*, 3663 – 3672; f) L. Carlucci, G. Ciani, D. M. Proserpio, S. Rizzato, *CrystEngComm* **2002**, *4*, 413 – 425.

[16] M. Scheer, L. J. Gregoriades, A. V. Virovets, W. Kunz, R. Neueder, I. Krossing, *Angew. Chem. Int. Ed.* **2006**, *45*, 5689 – 5693; *Angew. Chem.* **2006**, *118*, 5818 – 5822.

[17] For further details of the analytical data, see Supporting Information.

[18] T. Sakano, M. Okano, K. Osakada, *J. Inorg. Organomet. Polym. Mater.* **2009**, *19*, 35 – 45.

[19] The length of the linker in linear conformation was calculated with CHEM3D Ultra by PerkinElmer Informatics Inc., **2019** Version 19.1.08.

[20] The outer diameter of the supramolecular node was calculated as the distance of two outermost H atoms plus twice the van der Waals radius of H (0.11 nm according to R. S. Rowland, R. Taylor, *J. Phys. Chem.* **1996**, *100*, 7384 – 7391). The void dimensions were calculated as the minimum × maximum distances between two opposing P atoms minus twice the van der Waals radius of P (0.180 nm).

[21] a) M. A. Carvajal, J. J. Novoa, S. Alvarez, *J. Am. Chem. Soc.* **2004**, *126*, 1465 – 1477; b) E. Peresypkina, M. Bielmeier, A. V. Virovets, M. Scheer, *Chem. Sci.* **2020**, *11*, 9067 – 9071.

[22] M. Scheer, A. Schindler, J. Bai, B. P. Johnson, R. Merkle, R. Winter, A. V. Virovets, E. V. Peresypkina, V. A. Blatov, M. Sierka, H. Eckert, *Chem. Eur. J.* **2010**, *16*, 2092 – 2107.

[23] a) V. A. Blatov, A. P. Shevchenko, D. M. Proserpio, *Cryst. Growth Des.* **2014**, *14*, 3576 – 3586; b) V. A. Blatov, M. O'Keeffe, D. M. Proserpio, *CrystEngComm* **2010**, *12*, 44 – 48.

[24] a) N. Byrd, R. J. Bartlett, J. A. Montgomery, Jr., *J. Phys. Chem. A* **2014**, *118*, 1706 – 1712; b) N. O. B. Lüttschwager, T. N. Wassermann, R. A. Mata, M. A. Suhm, *Angew. Chem. Int. Ed.* **2013**, *52*, 463 – 466; *Angew. Chem.* **2013**, *125*, 482 – 485.

Manuscript received: March 3, 2021
Accepted manuscript online: March 8, 2021
Version of record online: May 1, 2021

